ACS OMEGA

http://pubs.acs.org/journal/acsodf
Article

Laser-Induced Graphene-Based Potentiometric pH and Nonenzymatic Uric Acid Sensors for Urine Analysis on Baby Diaper

Md Rasel, Sofia Rodrigues Teixeira, Jahidul Islam, Hassan Hamidi, Aidan J. Quinn, and Daniela Iacopino*

Cite This: *ACS Omega* 2026, 11, 25139−25148

ABSTRACT: The fabrication of wearable sensors and their integration into real devices is an emerging demand in the field of sensor development. In this work, flexible sensors based on laser-induced graphene (LIG) were developed using a low-cost visible laser on polyimide tape for pH and uric acid monitoring in urine. A potentiometric pH sensor was fabricated by modifying the LIG surface with polyaniline, achieving a sensitivity of 56.7 ± 2.6 mV/pH across a wide pH range (4−10) with a rapid response time of <10 s. The sensor exhibited high selectivity toward proton ions and maintained stable performance for 6 weeks without the need for preconditioning or special storage conditions. In parallel, a nonenzymatic uric acid sensor based on LIG exhibited strong selectivity against common interfering species, excellent reproducibility (RSD <1%), and a sensitivity of 116.4 μAdec^{-1}, with a limit of detection (LOD) of 35 μM (3S/N) in the concentration range of 0.05−0.6 mM in buffer solution. Both sensors maintained almost similar sensitivities in artificial urine samples, and their performance was successfully demonstrated in baby diapers using a portable potentiostat, highlighting their potential for miniaturized wearable health monitoring applications.

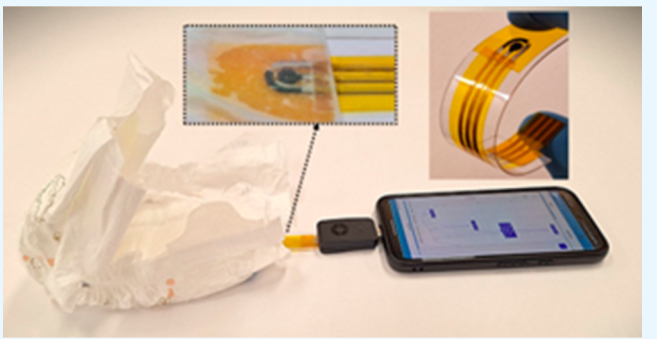

INTRODUCTION

Wearable biosensors are increasingly transforming personalized healthcare by enabling continuous, noninvasive, and real-time monitoring of physiological biomarkers.[1,2] Among the various biofluids explored for wearable sensing, urine represents a particularly rich yet underutilized source of information owing to its high analyte concentration, ease of collection, and clinical relevance to a wide range of metabolic and renal conditions. This makes urine-based sensing especially promising for applications in neonatal, elderly, and chronic disease care, where frequent and unobtrusive monitoring is critical.[3−5] Currently, commercial urine test strips are used as point-of-care diagnostic tools for the rapid detection of urinary tract infections.[6] However, these tests rely on the optical detection of colorimetric changes, which cannot provide real-time monitoring or integration with mobile devices. Moreover, optical detection methods are often limited in sensitivity and accuracy, particularly for low-concentration analytes.[7,8] In contrast, electrochemical sensing approaches such as potentiometry and voltammetry offer high sensitivity, operational simplicity, and compatibility with miniaturized, low-power platforms.[9,10] Several studies have already demonstrated successful detection of urinary biomarkers, including pH, electrolytes (e.g., K^+, Na^+), metabolites (e.g., uric acid, glucose), and therapeutic drugs, using materials such as metal oxides, conducting polymers, enzymes, and carbon-based nanomaterials.[11−14] Despite advances in wearable sensing, the integration of electrochemical biosensors into diapers remains largely underexplored. Most commercially available or prototype "smart diapers" are limited to moisture detection, providing an alert of urination events through resistive or capacitive sensors,[15,16] but do not enable quantitative biochemical analysis of urine. A few emerging studies have attempted to address this limitation. For instance, Isao *et al.* developed a self-powered diaper capable of glucose detection by utilizing urine glucose as a biofuel,[17] and Jiru *et al.* also reported a similar enzymatic biofuel cell-based system for urine glucose monitoring for diabetic patients.[18] Xiangling *et al.* demonstrated a multiplexed electrochemical sensor integrated into a diaper for glucose, H_2O_2, uric acid, sodium, and potassium ion detection using carbon nanotube-coated magnetron-sputtered gold electrodes.[19] However, such an approach required costly and complex fabrication steps,

Received: October 23, 2025
Revised: February 24, 2026
Accepted: February 25, 2026
Published: April 23, 2026

https://doi.org/10.1021/acsomega.5c11146
ACS Omega 2026, 11, 25139−25148

Scheme 1[a]

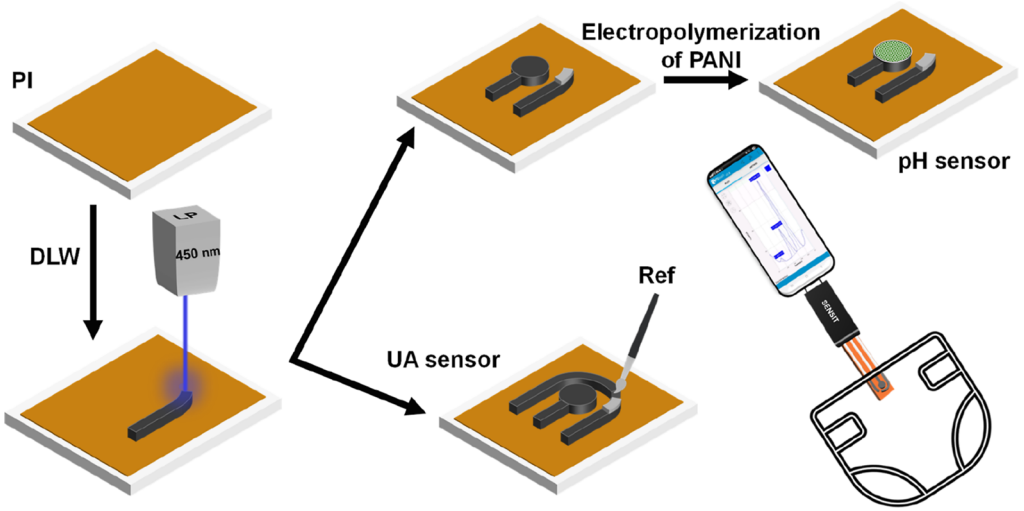

[a]Schematic representation of sensor fabrication using a visible laser by the direct laser writing(DLW) technique with subsequent modification steps including reference electrode painting (Ref) and electropolymerization of PANI (for the pH sensor) and demonstrating its potential application for real-time monitoring of pH and UA in a baby diaper.

including the use of enzymes and Pt nanoparticles. Huang *et al.* developed a diaper-integrated glucose and uric acid monitoring platform featuring wireless smartphone-based signal acquisition, employing screen-printed carbon ink electrodes on a PET substrate functionalized with glucose oxidase and urate oxidase enzymes.[20] Sohel *et al.* reported a nonenzymatic uric acid sensing platform in human urine based on a flexible stainless steel electrode modified with copper oxide-graphene oxide nanocomposite and integrated readout electronics.[21] However, the reported platform was not integrated into a diaper format, limiting its applicability for real-time, on-body urine monitoring. More recently, Natcha *et al.* reported a diaper-integrated sensor for K^+ and morphine detection in urine,[22] representing a notable advancement in diaper-based chemical sensing. Despite these developments, the electrochemical sensing of urine pH directly within a diaper has not yet been reported. This is a significant gap given that both urine pH and uric acid levels are critical indicators for assessing renal health and hydration status in neonates and infants.

Laser-induced graphene (LIG) has gained significant attention as a low-cost, scalable, and high-performance electrode material for flexible biosensing platforms. Produced by direct laser scribing of polyimide, LIG exhibits a porous 3D architecture that combines excellent electrical conductivity, mechanical flexibility, and large surface area, properties ideal for electrochemical detection in wearable formats.[23−26] Moreover, the LIG surface can be readily functionalized with conductive polymers, nanoparticles, enzymes, and antibodies, further enhancing analyte specificity and electrochemical response.[23,27−29] Despite its potential, only a single example of an LIG-based smart diaper report exists.[30] Furthermore, the integration of advanced sensing materials such as LIG and the evaluation of sensors under realistic conditions, such as embedding in a diaper matrix and monitoring sensor stability, response time, and interference, remain largely unexplored.

This work addresses these gaps by developing a flexible, LIG-based biosensor fabricated on polyimide for the detection of urinary pH and uric acid (Scheme 1 shows sensor fabrication and integration). The pH sensor was simply fabricated by modification of bare LIG with polyaniline. The uric acid sensor was solely based on bare LIG, leveraging its inherent electrocatalytic properties for sensitive voltammetric detection. The sensing platform was integrated into a diaper, and its performance was successfully validated using a portable potentiostat, with results comparable to those obtained from standard benchtop instruments. The system was designed with real-time wireless compatibility, highlighting its potential as a practical, low-cost, and scalable tool for personalized health monitoring through smart hygiene products.

EXPERIMENTAL SECTION

Reagents and Chemicals

Aniline, sulfuric acid, polyvinyl butyral (PVB), acetone, isopropyl alcohol, phosphate buffer saline (PBS) tablet, boric acid, phosphoric acid, acetic acid, uric acid, ascorbic acid, dopamine, glucose, potassium hexacyanoferrate (III) trihydrate, sodium chloride, potassium chloride, sodium sulfate, sodium citrate, creatinine, urea, calcium chloride, ammonium chloride, magnesium sulfate pentahydrate, sodium hydroxide, hydrochloric acid, potassium oxalate, sodium dihydrogen phosphate monohydrate, disodium hydrogen phosphate heptahydrate, and silver/silver chloride (60/40) paste were purchased from Sigma-Aldrich. Polyimide tape and silver conducting paste were purchased from Radionics Ireland. A microscopic glass slide (1.0 to 1.2 mm thickness) was purchased from the Fisher Scientific store in Ireland. A PET sheet (0.19 mm thickness) was purchased from Amazon UK. Baby Nappies (Lupilu brand, size 1) were purchased from the local store Lidl Ireland. All chemicals were analytical grade and used without any further treatment. Deionized water (18.3 MΩ·cm) from a Milli-Q System was used throughout. Preparation of Britton Robinson buffer solution and artificial urine is described in the Supporting Information.

Laser-Induced Graphene Electrode Fabrication

LIG electrodes were fabricated using a direct laser writing technique in two different patterns. The pH sensor design consisted of a circular indicator electrode (IE, 3 mm diameter) and a reference electrode (RE), while the uric acid design used a three-electrode configuration consisting of a circular working electrode (WE, 3 mm diameter), a counter electrode (CE), and a RE. These patterns were laser-written on the surface of a polyimide tape (approximately 70 μm thick) affixed to a glass slide (thickness 1 mm) and PET (thickness 190 μm)

https://doi.org/10.1021/acsomega.5c11146
ACS Omega 2026, 11, 25139−25148

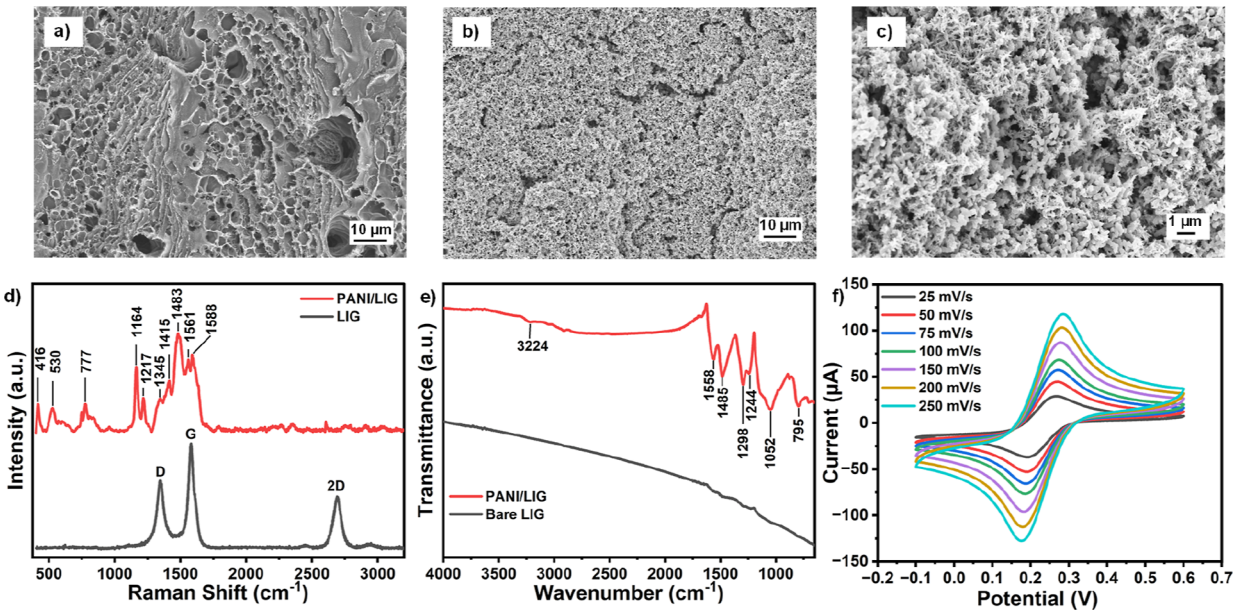

Figure 1. (a) SEM image of LIG; SEM of polyaniline-modified LIG with lower magnification (b) and higher magnification (c); (d) Raman spectra of bare LIG and PANI/LIG; (e) FTIR spectra of bare LIG and PANI/LIG; (f) cyclic voltammograms of bare LIG at different scan rates from 25 mVs^{-1} to 250 mVs^{-1} in 5 mM $Fe(CN)_6^{3-/4-}$ containing 0.1 M KCl.

sheet. For this purpose, a laser (Laser Pecker2 hand-held engraver) with a power of 5 W and an illumination wavelength of 450 nm was utilized. The optimization for laser writing settings is described in Figure S1. The values of optimum settings were a resolution of 2k, a defocusing distance of 5 mm, a laser power of 15% (of 5 W), and a depth (or writing speed) of 13%. To eliminate residual carbonaceous particles, the entire surface of the electrodes was sequentially washed with acetone, isopropyl alcohol, and deionized water after fabrication. Then, a drop of Ag/AgCl paste was applied on the surface of the RE and dried at 80 °C for about 10 min. Conductive silver paint was used on the LIG contact pads to ensure a good electrical connectivity. The nonactive area of the electrodes was insulated using nail varnish.

Fabrication of Nonenzymatic Uric Acid Biosensor and pH Sensor

A three-electrode-patterned LIG electrode was used for the nonenzymatic uric acid sensor without further modification. The pH sensor was fabricated by modifying the pH-indicating electrode with polyaniline. Polyaniline was electropolymerized on the LIG electrode (IE) in 0.1 M aniline and 1 M H_2SO_4 using cyclic voltammetry (CV) (−0.2 to 1.2 V, 7 scans) in a conventional three-electrode setup with an external Ag/AgCl (3 M KCl) as RE and Pt wire as CE.[31] Then, 5 μL of the cocktail mixture of PVB was drop-casted on the Ag/AgCl reference electrode. The cocktail mixture was prepared by dissolving 78.1 mg of PVB and 50 mg of NaCl in 1 mL of methanol.[32]

Characterizations

The surface morphology of LIG was examined by using scanning electron microscopy (SEM) (Zeiss SUPRA 35 VP, 5 kV). Raman spectra were acquired with a Horiba XploRA microscope employing a 532 nm, 70 mW laser source. Fourier transform infrared (FTIR) spectra were collected on a PerkinElmer Spectrum Two spectrometer in the 4000−450 cm^{-1} range, with a resolution of 4 cm^{-1}, averaged over 20 scans. The sheet resistance (R_{sh}) of LIG rectangular patterns (3 × 15 mm) was determined using a Fluke 179 true RMS multimeter. Electrochemical characterization, including potentiometric and voltammetric measurements, was carried out on an Autolab PGSTAT204 potentiostat (Metrohm, Utrecht, The Netherlands) configured with a three-electrode system. Sensor performance in baby diapers was further evaluated using a portable Sensit Smart smartphone-based potentiostat (PalmSens, Houten, The Netherlands).

RESULTS AND DISCUSSION

Laser-Induced Graphene (LIG) Sensors: Fabrication and Characterization

Electrical characterization of as-fabricated LIG sensors showed that the produced LIG materials are reproducible with a low sheet resistance (R_{sh}) equal to 13 Ωsq^{-1}. PANI was electropolymerized onto the LIG surface via cyclic voltammetry for pH sensing. To achieve complete and uniform coverage of the LIG electrode, electropolymerization was performed with different cycle numbers. At 5 cycles, only partial surface coverage was observed (Figure S2a), whereas 7 cycles produced a full coverage, less defective film. Increasing to 10 cycles led to crack formation (Figure S2b), likely caused by overgrowth and internal stress. Based on these results, 7 cycles were selected as the optimal conditions for sensor fabrication. The morphology of LIG and the optimized PANI/LIG electrode materials was characterized by scanning electron microscopy. Figure 1a shows SEM images of LIG, displaying the high surface area and high density of defects typical of laser-scribed graphitic materials.[33] The SEM image of PANI/LIG (Figure 1b) showed the uniform distribution of nanosponge-shaped electrodeposited polyaniline on the LIG surface. In the higher magnification SEM of PANI/LIG (Figure 1c), the interconnected morphology of PANI was clearly observed, confirming its homogeneous growth on the LIG electrode.

The Raman spectra of LIG and PANI/LIG are shown in Figure 1d. The spectrum of LIG exhibited the characteristic features of graphitic materials with D, G, and 2D peaks centered at 1347 cm^{-1} (defects in graphene), 1582 cm^{-1} (sp^2 carbon stretching), and 2692 cm^{-1} (second-order zone-boundary phonons), respectively. The I_D/I_G ratio of 0.78 indicated a significant degree of crystallinity within a disordered graphitic carbon network, while the I_{2D}/I_G ratio

https://doi.org/10.1021/acsomega.5c11146
ACS Omega 2026, 11, 25139−25148

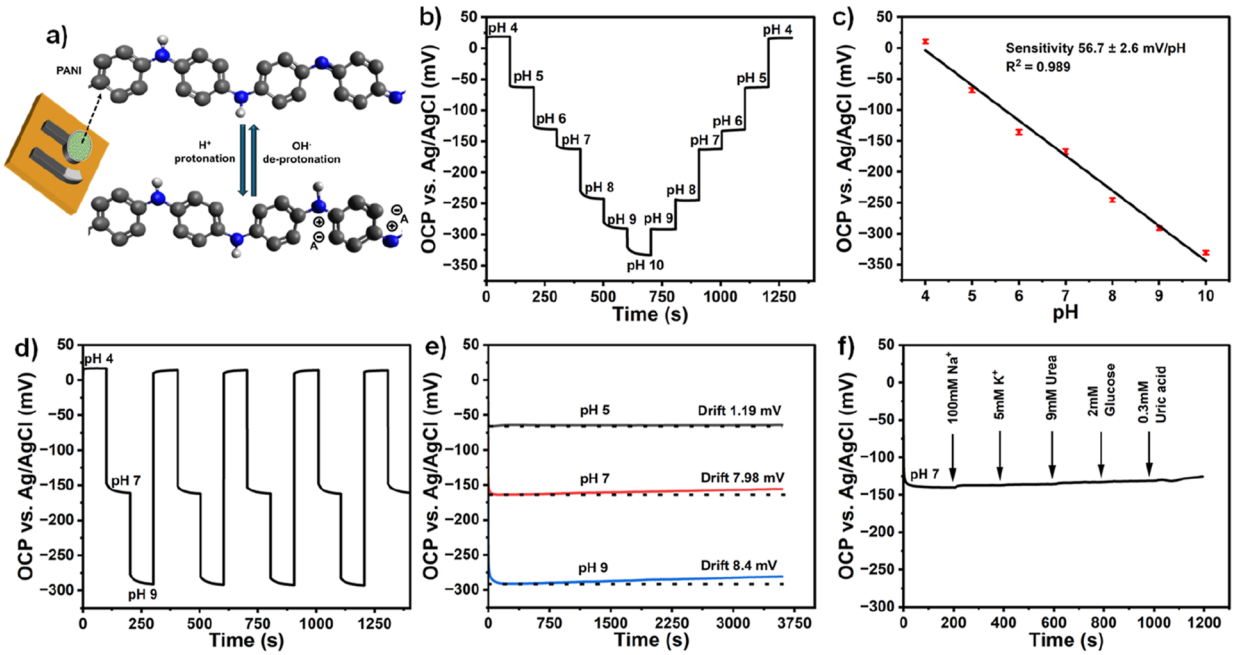

Figure 2. (a) Schematic mechanism of the pH sensor; (b) open circuit potential (OCP) response of the pH sensor during stepwise pH variation from 4 to 10 followed by from 10 to 4; (c) corresponding calibration curve of the pH sensor (n = 6); (d) the response of the pH sensor in pH 4, 7, and 9 and its recovery capability; (e) long-term stability of the pH sensor for continuous 1 h measurement in acidic (pH 5), neutral (pH 7), and basic (pH 9) pH buffer conditions; (f) interference test of the pH sensor at pH 7.

of 0.65 reflected the presence of multilayer graphene structures.[34] The Raman spectrum of PANI/LIG revealed several new peaks, providing clear evidence of the formation of PANI on the LIG surface. In the low-frequency region, bands around 416 and 530 cm^{-1} corresponded to ring deformation vibrations, while features observed between 750 and 1000 cm^{-1} were attributed to C−H out-of-plane and in-plane bending modes. Additional bands at 1164 and 1217 cm^{-1} were associated with C−H bending and C−N stretching within quinonoid units. At higher frequency, characteristic bands appeared at approximately 1345, 1483, and 1588 cm^{-1}, corresponding to C−N^+ stretching of polaronic species, C═N vibrations of quinonoid rings, and C═C stretching in quinoid and benzenoid structures, respectively. These spectral features confirmed both the structural integrity and the successful deposition of conductive PANI on the LIG surface.[35] FTIR analysis was employed to examine the infrared absorption characteristics of LIG and PANI/LIG, as shown in Figure 1e. The LIG sample (the black spectrum) was featureless, thus confirming the conversion of polyimide into graphitic carbon.[36] In contrast, the PANI/LIG spectrum (red spectrum) exhibited distinct absorption bands, indicating successful PANI formation. The peak at 795 cm^{-1} corresponded to out-of-plane C−H bending of the aromatic ring,[37] while the peak at 1052 cm^{-1} with its shoulder was assigned to N═Q═N stretching. Additional peaks at 1558 cm^{-1}, 1485 cm^{-1}, and 1244 cm^{-1} corresponded to C═C and C−N vibrations of quinoid and benzenoid structures in PANI.[38] The broad absorption at 3224 cm^{-1} was attributed to the N−H group. The appearance of PANI-specific peaks in the PANI/LIG spectrum confirmed their successful electrochemical polymerization on the LIG surface.

The electrochemical behavior of LIG was investigated by cyclic voltammetry using the three-electrode design shown in Figure 1f. The CVs recorded at different scan rates (25−250 mVs^{-1}) in a 5 mM ferricyanide solution displayed the characteristic anodic and cathodic peaks of the $Fe(CN)_6^{3-/4}$ redox couple. The anodic peak current increases with the square roots of the scan rates (Figure S3a), with a correlation coefficient (R^2) of 0.99, indicating the system is diffusion-controlled. At a scan rate (ν) of 100 mVs^{-1} the anodic−cathodic peak separation potential was 81 mV, indicating quasi-reversible electron transfer. The sensor showed the same response after 25 consecutive scans in ferricyanide solution (Figure S3b), demonstrating its electrochemical stability and suitability for electrochemical sensor applications.

Characterization of the pH Sensor

The working principle of the as-fabricated potentiometric pH sensor (Figure 2a) is based on reversible protonation and deprotonation of the PANI-modified LIG electrode in acidic or basic environments. The resulting charge accumulation generates a potential that is measured against an Ag/AgCl reference electrode (RE) under open-circuit conditions (OCP) and can be correlated with the pH value. Figure 2b shows the OCP vs time profile of the fabricated pH sensor in Britton Robinson buffer solutions, where the pH was sequentially increased from 4 to 10 and then decreased back to 4, covering the physiologically relevant urine range. The sensor exhibited a rapid response, reaching a stable OCP value within 10 s after each pH change. The sensor exhibited a linear Nernstian response with a good sensitivity and regression coefficient (R^2) of 56.7 ± 2.6 mV/pH and 0.989 (n = 6), respectively, as plotted in Figure 2c. Based on the sensitivity and its uncertainty ($\Delta V/S$), the minimum detectable pH change (resolution) was estimated to be approximately 0.05 pH. This data was obtained from six independently fabricated sensors, representing the reproducibility of the sensor performance. The repeatability and recovery performance of the pH sensor were assessed under three representative conditions: acidic (pH 4), neutral (pH 7), and basic (pH 9) continuous

https://doi.org/10.1021/acsomega.5c11146
ACS Omega 2026, 11, 25139−25148

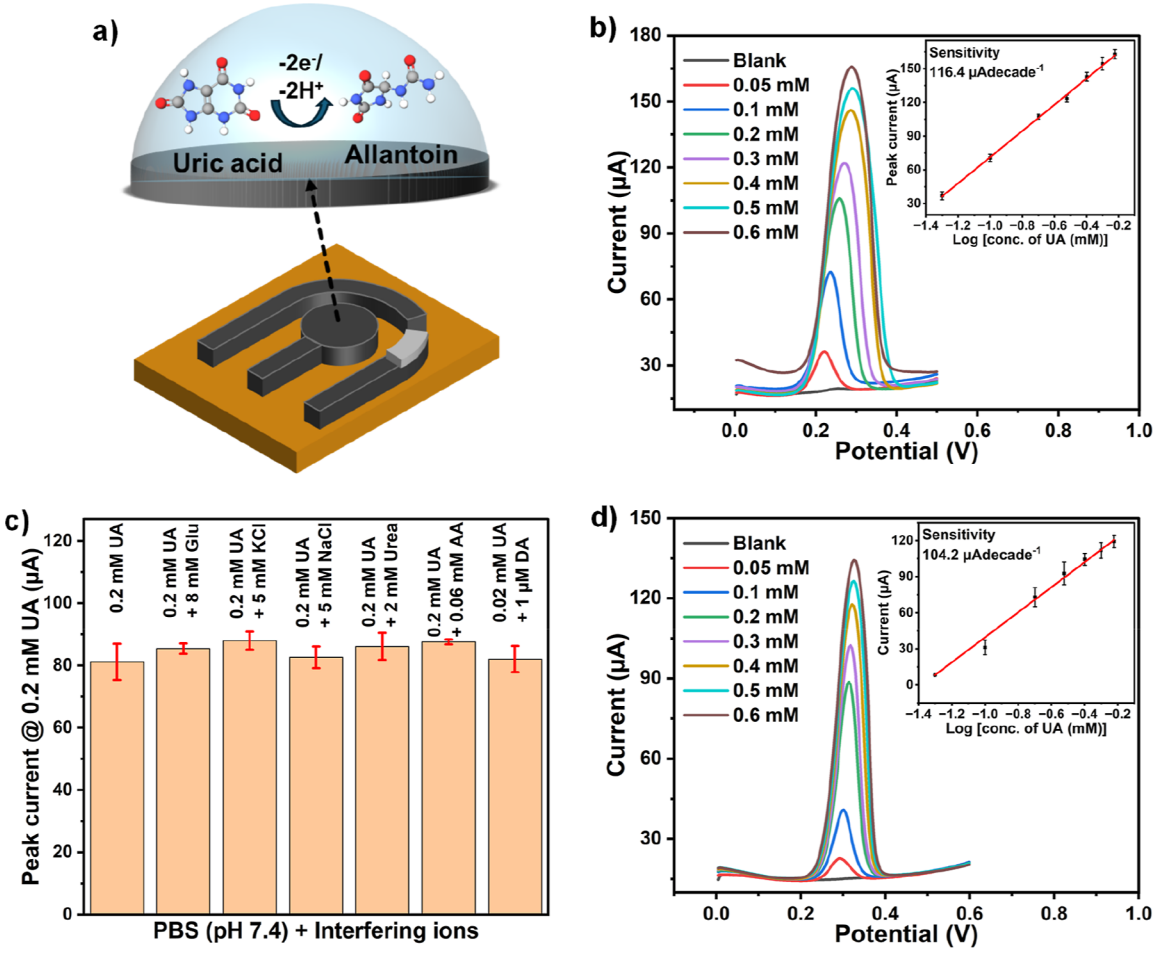

Figure 3. (a) Schematic diagram showing the mechanism of uric acid detection on LIG; (b) SWV of uric acid at different concentrations in PBS solution. Inset: corresponding calibration curve; (c) interference test of the UA sensor in the presence of relevant concentrations of glucose, KCl, NaCl, urea, AA, and DA at 0.2 mM UA; (d) SWV of UA at different concentrations in artificial urine. Inset: corresponding calibration curve.

conditions, as shown in Figure 2d. After four successive cycles, the pH sensor yielded an average sensitivity of 57.80 mV/pH, which is almost similar to its initial sensitivity, demonstrating the excellent repeatability of the developed sensor. Additionally, the hysteresis of the sensor after four cycles was calculated to be less than 1 mV for pH 4, 7, and 9, further confirming the stable and reliable performance of the developed sensor. The stability of the fabricated pH sensor was evaluated by immersing the sensors at the different pH conditions (5, 7, and 9); the changes in the OCP values were observed over stipulated time intervals. As evident in Figure 2e, the sensor showed a stable OCP response over an hour period with a drift of less than 10 mV, where for acidic, neutral, and basic conditions, it was 1.19, 7.98, and 8.4 mV, respectively, indicating the excellent stability of the sensor for the urine pH measuring application. The selectivity of the fabricated pH sensor at neutral pH was investigated in the presence of other species related to urine, including Na^+, K^+, urea, glucose, and uric acid. As shown in Figure 2f, the sensor displayed an insignificant response for other species, thanks to the effective coating of the proton-sensitive PANI membrane on the IE. For the long-term stability test, three pH sensors were chosen randomly and tested in buffer solutions with pH ranging from 4 to 10 for 6 weeks without any preconditioning or specific storage conditions. The sensor showed almost similar sensitivity throughout the study, showing only an average decrease of 0.46% from its first week's sensitivity after 6 weeks. Detailed results for each sensor at each time point are provided in Supporting Information Table S1.

Characterization of the Uric Acid Sensor

Uric acid (UA) is a diprotic compound with dissociation constants (pK_{a_1} = 5.4 and pK_{a_2} = 9.8), existing mainly in the form of urate ions under conditions above these values.[39] The molecular structure of UA is illustrated in Figure 3a, together with the mechanism of electrochemical detection on LIG electrodes, involving UA oxidation into allantoin by transfer of 2 protons and 2 electrons.[40,41] Figure 3b reports the direct electrocatalytic oxidation of UA at LIG electrodes measured by SWV over a range of UA concentrations from 0.05 to 0.6 mM in 0.01 M PBS (pH 7.4). In the absence of UA, no peak was observed in the voltammogram, whereas a sequential increase in oxidative peak current was observed with increasing UA concentrations. The calibration curve showed a well-defined linear relationship between peak current and the logarithm of uric acid concentration within the range of 0.05 mM−0.6 mM (inset of Figure 3b). The limit of detection (LOD) was determined to be 0.035 mM, calculated using the standard equation LOD = 3.3*σ/S, where σ denotes the standard deviation of the blank response and S corresponds to the slope of the calibration curve.[42] The LOD obtained for this nonenzymatic LIG UA sensor is higher than that reported

https://doi.org/10.1021/acsomega.5c11146
ACS Omega 2026, 11, 25139−25148

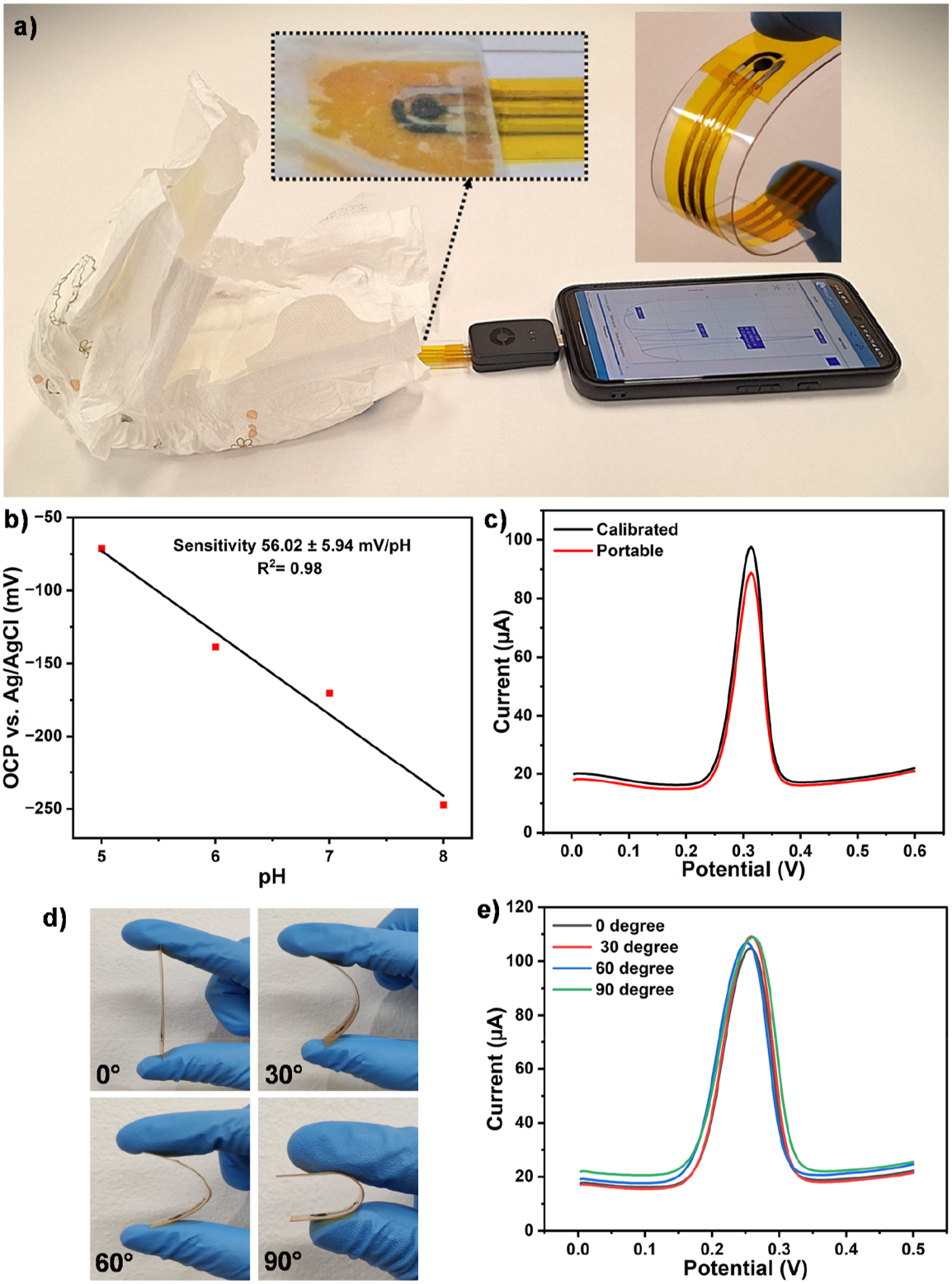

Figure 4. (a) UA flexible sensor integrated into a baby diaper with Sensit Smart portable potentiostat; (b) calibration curve of the pH sensor OCP response in the pH range 5−8 within the baby diaper environment; (c) comparison of SWV responses of the UA sensor in artificial urine containing 0.2 mM uric acid, measured using the portable potentiostat and a standard calibrated system; (d) images of the LIG sensor under different mechanical bending conditions; (e) SWV of the UA sensor at 0.2 mM UA under different bending conditions.

for some LIG sensors, such as LIG sensors scribed on polyimide modified with Pt nanoparticles (0.22 μM)[43] and NiO−$Ti_3C_2T_x$ nanosheets (0.08 μM).[44] However, it is important to note that extremely low LOD is not mandatory for UA detection and quantification in baby urine, since the physiologically relevant concentrations are above 0.1 mM.[30,45,46] In urine, UA exists at considerably higher concentrations owing to the presence of proteins and other

https://doi.org/10.1021/acsomega.5c11146
ACS Omega 2026, 11, 25139−25148

Table 1. A Comparison Table Summarizing Performance Relative to Existing LIG-Based pH and UA Sensors[a]

Modification materials	Laser type	Linear range	LOD	Sensitivity	Detection environment	Ref.
pH sensor						
PANI/LIG	CO_2	4−8	_	58.25 mV/pH	urine	30
PANI/MXene/LIG/PDMS	CO_2	4−9	_	57.03 mV/pH	wound exudate	51
Riboflavin	CO_2	2.81−7.82	_	56 mV/pH	wound care	52
PANI/LIG	CO_2	4−7	_	51.5 mV/pH	sweat	53
PANI/LIG	visible	4−10	_	56.7 ± 2.6 mV/pH	artificial urine	**This work**
Uric acid sensor						
GO/AuNPs/LIG	CO_2	0.1−0.6 mM	21.4 μM	17.80 μA/mM	urine	30
MXene/LIG/PDMS	CO_2	50−1200 μM	50 μM	422.5 $\mu AmM^{-1}cm^{-2}$	wound exudate	51
Paper-LIG	CO_2	0.01−0.250 mM	3.97 μM	0.363 μAcm^{-2} μM^{-1}	urine	10
CoNCs/LIG	CO_2	5−700 μM	3.66 μM	6.75 $\mu A\mu M^{-1}$ cm^{-2}	PBS	54
BSAT/LIG	visible	20−1000 μM	2.1 μM	_	saliva	55
LIG	CO_2	3−200 μM	0.28 μM	6.49 $\mu A\mu M^{-1}$ cm^{-2}	sweat	56
rGO/AgCo/LIG	CO_2	0.1−2000 μM	3.75 μM	1.76 $\mu A\mu M^{-1}$ cm^{-2}	PBS	57
Paper-LIG	CO_2	1−1000 μM	41 nM	24.35b ± 1.55 μA μM^{-1}	PBS	24
C−Au-LIG	CO_2	0−100 μM	0.5 μM	3.11 $\mu A\mu M^{-1}$ cm^{-2}	sweat	27
LIG	visible	0.05−0.6 mM	35 μM	116.4 $\mu Adec^{-1}$	artificial urine	**This work**

[a]PANI, polyaniline; GO, graphene oxide; AuNPs, gold nanoparticles; CoNCs, cobalt nanostructures; BSAT, bovine serum albumin tween-20 layer; rGO/AgCo, reduced graphene oxide silver cobalt nanocomposite; C−Au-LIG, chitosan gold clusters on LIG.

solubilizing compounds.[47,48] Furthermore, pH and temperature also play an effective role in the solubility of UA.[49] Indeed, the LIG electrodes provide a linear response toward UA in the concentration range of 0.05−0.6 mM UA, which represents a wide and practically useable range suitable for analysis of baby urine samples, which covers the 0.1−0.5 mM range taken as reference values encountered in real, nondiluted baby urine.[10,30,45,46] Furthermore, the straightforward and environmentally friendly fabrication process yields low-cost sensing units with a sensitivity of 116.4 $\mu Adec^{-1}$ at pH 7.4, exceeding several enzymatic and nonenzymatic UA sensors previously reported with more complex and expensive production methods.[10,50] In contrast, previously reported CO_2 laser-scribed polyimide LIG-based UA sensors exhibited a substantially narrower linear detection range (limited to concentrations below 20 μM) and were not evaluated in biological fluids.[43] The selectivity of the fabricated UA sensor was evaluated to ensure its applicability for UA detection in complex biological samples, such as urine. To assess interference effects, SWV studies were carried out in the presence of 0.2 mM UA by adding potential interfering species, including 8 mM glucose (Glu), 5 mM potassium chloride (KCl), 5 mM sodium chloride (NaCl), 2 mM urea, 0.06 mM ascorbic acid (AA), and 1 μM dopamine (DA), as shown in Figure S4. Figure 3c presents the error bars of the UA oxidation current recorded for 0.2 mM UA in the presence of these interferents. As shown in Figure 3c, the presence of interfering species resulted in a minor increase in the UA oxidative peak current (4.2, 6.8, 1.5, 4.9, 6.4, and 0.9 μA for Glu, KCl, NaCl, urea, AA, and DA, respectively). These data represent that the sensor exhibits acceptable selectivity toward common interfering ions and components present in urine, as all relative changes for the UA oxidation peak current are less than 10%. Finally, the sensor was tested in artificial urine by spiking different concentrations of UA ranging from 0.05 mM to 0.6 mM, as shown in Figure 3d. The sensor showed a very good linear response in artificial urine with a sensitivity of 104.2 $\mu Adec^{-1}$ (inset of Figure 3d). Considering that the artificial urine contains electrolytes and protein complexes, the sensor showed a slightly lower variation compared to the response observed in PBS for three randomly chosen sensors. Nevertheless, all these results demonstrate the potential of the nonenzymatic uric acid sensor in terms of sensitivity, detection range, and LOD, highlighting its potential as a cost-effective and efficient platform for UA detection.

Application of the Wearable Sensing System

To demonstrate the system function under realistic conditions, the pH and UA sensors were integrated into a baby diaper (Figure 4a). The flexible pH sensor was first connected to the Sensit Smart smartphone-based potentiostat and inserted into the absorbent layer of the diaper. Artificial urine solutions with varying pH values (5−8) were then sequentially introduced to assess the sensor's OCP response. The sensor exhibited a sensitivity of 56.02 ± 5.94 mV/pH, closely matching the sensitivity obtained in Britton−Robinson buffer (57.80 mV/pH), confirming its reliable functionality for urine-based pH monitoring within the diaper. For continuous pH monitoring in baby urine, the sensor was immersed in artificial urine (pH 6) to evaluate the pH drift arising from the presence of the interfering species in the artificial urine. The OCP response of the sensor is shown in Figure S5a. The sensor exhibited a potential drift of approximately 5 mV/h, indicating good stability under continuous exposure to artificial urine. To assess sensor performance under repetitive wetting events that mimic a single diaper use time, artificial urine solution (pH 6) was added to the diaper three times at a time interval of 5 min, and the corresponding OCP response was recorded. Figure S5b shows the OCP value represents that the sensor shows an acceptable level of drift, comparable to the response observed in artificial urine without diaper conditions. These results confirm that the sensor maintains a stable performance under repeated wetting events, supporting its suitability for practical diaper-based pH monitoring. Afterward, artificial urine containing 0.2 mM UA was added to the diaper to evaluate the response of the UA sensor using the SWV technique. The measured current corresponded well with the calibration curve established in artificial urine, validating the robustness and accuracy of the detection. Mechanical bendability of the sensor is essential for a wearable application. To evaluate this

https://doi.org/10.1021/acsomega.5c11146
ACS Omega 2026, 11, 25139−25148

property, the sensor was tested under three mechanical bending conditions (30°, 60°, and 90°), as illustrated in Figure 4d. The CV curves recorded in 5 mM $[Fe(CN)_6]^{3-/4-}$ containing 0.1 M KCl (Figure S6) show only a slight impact of mechanical deformation on electrochemical response. The redox probe exhibits stable current signals with an RSD of 4.2% in CV measurements, even when the sensing chip is bent to 90°. Furthermore, the SWV of the UA sensor at 0.2 mM UA under different bent conditions is shown in Figure 4e. The UA oxidation peak currents remain nearly unchanged, yielding an RSD of 1.75%, indicating a reliable sensing performance under mechanical deformation. Thus, this LIG-based sensing platform is robust to mechanical deformation in wearable sensing applications and enables a stable and accurate signal readout. A comparison of the sensing performance of the proposed sensor with previously reported LIG-based pH and uric acid sensors is summarized in Table 1. Overall, these results demonstrate that the LIG-based sensing platform possesses excellent mechanical stability and shows promising potential for the reliable operation of both pH and uric acid sensors within a real diaper platform.

CONCLUSIONS

We have reported the fabrication and characterization of a flexible, wearable biosensing platform based on polyimide-LIG for real-time, noninvasive monitoring of urinary biomarkers. The pH sensor, modified with polyaniline, demonstrated a selective potentiometric response with a wide detection range, including physiological pH levels. In parallel, UA detection was demonstrated on an enzyme-free UA sensor, leveraging the intrinsic electrocatalytic properties of unmodified LIG for effective detection via voltammetric techniques. To evaluate the practical applicability, the sensor array was integrated into a diaper and tested using a portable potentiostat, where it exhibited stable and reliable performance. This approach offers a convenient solution for on-site urine monitoring, which is particularly beneficial for neonatal care. Further improvements can be made by enhancing the system's integration with compact electronics to enable seamless, real-time wireless data transmission to smart devices, supporting continuous and remote health monitoring. Overall, this study underscores the potential of integrating multiple electrochemical sensors into smart hygiene products, paving the way for personalized and continuous health monitoring.

ASSOCIATED CONTENT

Supporting Information

The Supporting Information is available free of charge at https://pubs.acs.org/doi/10.1021/acsomega.5c11146.

Additional text, figures, and tables, including solution preparation; optimization of laser instrumental settings and corresponding plots; SEM images of polyaniline-deposited LIG electrodes (5 cycles and 10 cycles); anodic peak current vs square root of the scan rate curve of the bare LIG sensor; cyclic voltammograms of bare LIG for 25 continuous cycles; SWV of uric acid in the presence of interfering species; OCP response of the pH sensor in artificial urine (pH 6) for 1 h; OCP response of the pH sensor in the repeated wetting even inside of the diaper for 17 min; cyclic voltammograms of bare LIG electrodes under different mechanical bending conditions; and summary of the long-term stability of pH sensors for 6 weeks (PDF)

AUTHOR INFORMATION

Corresponding Author

Daniela Iacopino − *Tyndall National Institute, University College Cork, Cork T12 R5CP, Ireland;* orcid.org/0000-0003-2301-9401; Email: daniela.iacopino@tyndall.ie

Authors

Md Rasel − *Tyndall National Institute, University College Cork, Cork T12 R5CP, Ireland;* orcid.org/0009-0001-7135-6675

Sofia Rodrigues Teixeira − *Tyndall National Institute, University College Cork, Cork T12 R5CP, Ireland;* orcid.org/0000-0002-3527-4816

Jahidul Islam − *Tyndall National Institute, University College Cork, Cork T12 R5CP, Ireland*

Hassan Hamidi − *Tyndall National Institute, University College Cork, Cork T12 R5CP, Ireland;* orcid.org/0000-0002-7775-8536

Aidan J. Quinn − *Tyndall National Institute, University College Cork, Cork T12 R5CP, Ireland;* orcid.org/0000-0003-4021-9990

Complete contact information is available at: https://pubs.acs.org/10.1021/acsomega.5c11146

Notes

The authors declare no competing financial interest.

ACKNOWLEDGMENTS

The authors gratefully acknowledge Rachel Breen and Gillian Collins for their assistance with the FTIR spectrum of LIG and PANI-modified LIG. This publication has emanated from research conducted with the financial support of the Research Ireland under the European Regional Development Fund Grant Number 13/RC/2077-P2 (CONNECT) and Horizon Europe projects GreenArt (101060941) and Herit4ages (101123175).

REFERENCES

(1) Kim, J.; Campbell, A. S.; de Ávila, B. E. F.; Wang, J. Wearable biosensors for healthcare monitoring. *Nat. Biotechnol.* **2019**, *37* (4), 389−406.

(2) Duan, H.; Peng, S.; He, S.; Tang, S. Y.; Goda, K.; Wang, C. H.; Li, M. Wearable electrochemical biosensors for advanced healthcare monitoring. *Adv. Sci.* **2025**, *12* (2), 2411433−28.

(3) Liu, R.; Nie, Q.; Wang, Y.; Wu, Y.; Tu, Y.; Xie, C.; Xiao, X.; You, R.; Lu, Y. Diaper-based wearable SERS sensing system with a silver nano dual-structure composite hydrogel for the detection of biomarkers and pH in urine. *Chem. Eng. J.* **2024**, *498*, 155207.

(4) Linh, V. T. N.; Lee, M. Y.; Mun, J.; Kim, Y.; Kim, H.; Han, I. W.; Park, S. G.; Choi, S.; Kim, D. H.; Rho, J.; Jung, H. S. 3D plasmonic coral nanoarchitecture paper for label-free human urine sensing and deep learning-assisted cancer screening. *Biosens. Bioelectron.* **2023**, *224*, 115076.

(5) Bi, Y.; Sun, M.; Wang, J.; Zhu, Z.; Bai, J.; Emran, M. Y.; Kotb, A.; Bo, X.; Zhou, M. Universal fully integrated wearable sensor arrays for the multiple electrolyte and metabolite monitoring in raw sweat, saliva, or urine. *Anal. Chem.* **2023**, *95* (16), 6690−6699.

(6) Gehringer, C.; Regeniter, A.; Rentsch, K.; Tschudin-Sutter, S.; Bassetti, S.; Egli, A. Accuracy of urine flow cytometry and urine test

strip in predicting relevant bacteriuria in different patient populations. *BMC Infect. Dis.* **2021**, *21* (1), 209.
(7) Kaur, B.; Kumar, S.; Kaushik, B. K. Novel wearable optical sensors for vital health monitoring systems—a review. *Biosensors* **2023**, *13* (2), 181.
(8) Wang, J.; Luo, Y.; Zhou, Z.; Xiao, J.; Xu, T.; Zhang, X. Epidermal wearable optical sensors for sweat monitoring. *Commun. Mater.* **2024**, *5*, 77.
(9) Dinasekaran, D.; John, J. F.; Subashchandran, S. Electrochemical sensing of uric acid: methods and recent materials. *J. Electrochem. Soc.* **2024**, *171*, 57505.
(10) Kulyk, B.; Pereira, S. O.; Fernandes, A. J. S.; Fortunato, E.; Costa, F. M.; Santos, N. F. Laser-induced graphene from paper for non-enzymatic uric acid electrochemical sensing in urine. *Carbon* **2022**, *197*, 253−263.
(11) Mohan, B.; Asif, M. B.; Pombeiro, A. Engineered conductive metal-organic frameworks for electrochemical detection of urinary biomarkers. *Small* **2024**, *21* (4), 2406222.
(12) Wang, G.; Han, R.; Li, Q.; Han, Y.; Luo, X. Electrochemical biosensors capable of detecting biomarkers in human serum with unique long-term antifouling abilities based on designed multifunctional peptides. *Anal. Chem.* **2020**, *92* (10), 7186−7193.
(13) Manikandan, R.; Jang, H. G.; Kim, C. S.; Yoon, J. H.; Lee, J.; Paik, H. J.; Chang, S. C. Nano-engineered paper-based electrochemical biosensors: versatile diagnostic tools for biomarker detection. *Coord. Chem. Rev.* **2025**, *523*, 216261.
(14) Bollella, P.; Fusco, G.; Tortolini, C.; Sanzó, G.; Favero, G.; Gorton, L.; Antiochia, R. Beyond graphene: electrochemical sensors and biosensors for biomarkers detection. *Biosens. Bioelectron.* **2017**, *89*, 152−166.
(15) Hu, M.; Lim, J. W.; Yap, P.; Ha, N.; Yeo, P. S.; Xu, G.; Deng, R.; Wee, S.; Ying, J. Smart diapers: from wetness monitoring to early diagnosis. *Appl. Phys. Rev.* **2025**, *12* (1), 011317.
(16) Tanweer, M.; Monga, D. C.; Gillan, L.; Sepponen, R.; Tanzer, I. O.; Halonen, K. A. I.; Tanweer, M.; Tanzer, I. Smart diaper with printed capacitive sensors and integrated front-end to monitor voided fluid volume. *IEEE Sens. J.* **2024**, *24*, 14443−14453.
(17) Shitanda, I.; Fujimura, Y.; Takarada, T.; Suzuki, R.; Aikawa, T.; Itagaki, M.; Tsujimura, S. Self-powered diaper sensor with wireless transmitter powered by paper-based biofuel cell with urine glucose as fuel. *ACS Sens.* **2021**, *6* (9), 3409−3415.
(18) Zhang, J.; Liu, J.; Su, H.; Sun, F.; Lu, Z.; Su, A. A wearable self-powered biosensor system integrated with diaper for detecting the urine glucose of diabetic patients. *Sens. Actuators B Chem.* **2021**, *341*, 130046.
(19) Li, X.; Zhan, C.; Huang, Q.; He, M.; Yang, C.; Yang, C.; Huang, X.; Chen, M.; Xie, X.; Chen, H. J. Smart diaper based on integrated multiplex carbon nanotube-coated electrode array sensors for in situ urine monitoring. *ACS Appl. Nano Mater.* **2022**, *5* (4), 4767−4778.
(20) Su, H.; Sun, F.; Lu, Z.; Zhang, J.; Zhang, W.; Liu, J. A wearable sensing system based on smartphone and diaper to detect urine in-situ for patients with urinary incontinence. *Sens. Actuators B Chem.* **2022**, *357*, 131459.
(21) Chaus, S. S.; Lal, S.; Bahubalindruni, P. G. A flexible and highly sensitive non-enzymatic electrochemical sensing platform with readout electronics for sensing uric acid in human urine: towards devices. *Electrochim. Acta* **2025**, *539*, 147114.
(22) Rasitanon, N.; Sangsudcha, W.; Jeerapan, I. A diaper-based printed sensing array for noninvasively and speedily detecting morphine and potassium ions. *Chem. Eng. J.* **2024**, *485*, 148898.
(23) Wan, Z.; Nguyen, N.; Gao, Y.; Li, Q. Laser induced graphene for biosensors. *Sustain. Mater. Technol.* **2020**, *25*, No. e00205.
(24) Bhattacharya, G.; Fishlock, S.; Hussain, S.; Choudhury, S.; Xiang, A.; Kandola, B.; Pritam, A.; Soin, N.; Roy, S.; McLaughlin, J. Disposable paper-based biosensors: optimizing the electrochemical properties of laser-induced graphene. *ACS Appl. Mater. Interfaces* **2022**, *14*, 31109−31120.
(25) Lahcen, A.; Rauf, S.; Beduk, T.; Durmus, C.; Aljedaibi, A.; Timur, S.; Alshareef, H.; Amine, A.; Wolfbeis, O.; Salama, K. Electrochemical sensors and biosensors using laser-derived graphene: a comprehensive review. *Biosens. Bioelectron.* **2020**, *168*, 112565.
(26) Yoon, H.; Nah, J.; Kim, H.; Ko, S.; Sharifuzzaman, Md.; Barman, S.; Xuan, X.; Kim, J.; Park, J. A chemically modified laser-induced porous graphene based flexible and ultrasensitive electrochemical biosensor for sweat glucose detection. *Sens. Actuators B Chem.* **2020**, *311*, 127866.
(27) Zhang, L.; Wang, L.; Li, J.; Cui, C.; Zhou, Z.; Wen, L. Surface engineering of laser-induced graphene enables long-term monitoring of on-body uric acid and pH simultaneously. *Nano Lett.* **2022**, *22* (13), 5451−5458.
(28) Yagati, A.; Behrent, A.; Beck, S.; Rink, S.; Goepferich, A.; Min, J.; Lee, M.-H.; Baeumner, A. Laser-induced graphene interdigitated electrodes for label-free or nanolabel-enhanced highly sensitive capacitive aptamer-based biosensors. *Biosens. Bioelectron.* **2020**, *164*, 112272.
(29) Vivaldi, F.; Dallinger, A.; Bonini, A.; Poma, N.; Sembranti, L.; Biagini, D.; Salvo, P.; Greco, F.; Di Francesco, F. Three-dimensional (3d) laser-induced graphene: structure, properties, and application to chemical sensing. *ACS Appl. Mater. Interfaces* **2021**, *13*, 30245−30260.
(30) Zhang, Y.; Tan, W.; Hu, X.; Pan, W.; Xu, T.; Wang, L.; Liu, C. Integrated smart diaper for self-pumping urine drainage and comfortable on-site electroanalysis. *Sens. Actuators B Chem.* **2026**, *446*, 138627.
(31) Wang, C.; Fan, K.; Shirzaei Sani, E.; Lasalde-Ramírez, J. A.; Heng, W.; Min, J.; Solomon, S. A.; Wang, M.; Li, J.; Han, H.; Kim, G.; Shin, S.; Seder, A.; Shih, C.-D.; Armstrong, D. G.; Gao, W. A microfluidic wearable device for wound exudate management and analysis in human chronic wounds. *Sci. Transl. Med.* **2025**, *17* (795), No. eadt0882.
(32) Guinovart, T.; Valdés-Ramírez, G.; Windmiller, J. R.; Andrade, F. J.; Wang, J. Bandage-based wearable potentiometric sensor for monitoring wound pH. *Electroanalysis* **2014**, *26* (6), 1345−1353.
(33) Vaughan, E.; Larrigy, C.; Burke, M.; Sygellou, L.; Quinn, A. J.; Galiotis, C.; Iacopino, D. Visible laser scribing fabrication of porous graphitic carbon electrodes: morphologies, electrochemical properties, and applications as disposable sensor platforms. *ACS Appl. Electron. Mater.* **2020**, *2* (10), 3279−3288.
(34) Tiliakos, A.; Ceaus, C.; Iordache, S. M.; Vasile, E.; Stamatin, I. Morphic transitions of nanocarbons via laser pyrolysis of polyimide films. *J. Anal. Appl. Pyrolysis* **2016**, *121*, 275−286.
(35) Trchová, M.; Morávková, Z.; Bláha, M.; Stejskal, J. Raman spectroscopy of polyaniline and oligoaniline thin films. *Electrochim. Acta* **2014**, *122*, 28−38.
(36) Imbrogno, A.; Islam, J.; Santillo, C.; Castaldo, R.; Sygellou, L.; Larrigy, C.; Murray, R.; Vaughan, E.; Hoque, M. K.; Quinn, A. J.; Iacopino, D. Laser-induced graphene supercapacitors by direct laser writing of cork natural substrates. *ACS Appl. Electron. Mater.* **2022**, *4* (4), 1541−1551.
(37) Trchová, M.; Stejskal, J. Polyaniline: The infrared spectroscopy of conducting polymer nanotubes (IUPAC technical report). *Pure Appl. Chem.* **2011**, *83* (10), 1803−1817.
(38) Feng, X. M.; Li, R. M.; Ma, Y. W.; Chen, R. F.; Shi, N. E.; Fan, Q. L.; Huang, W. One-step electrochemical synthesis of graphene/polyaniline composite film and its applications. *Adv. Funct. Mater.* **2011**, *21* (15), 2989−2996.
(39) Chong, D. P. Theoretical study of uric acid and its ions in aqueous solution. *J. Theor. Comput. Sci.* **2016**, *1* (1), 10−4172.
(40) Lakshmi, D.; Whitcombe, M. J.; Davis, F.; Sharma, P. S.; Prasad, B. B. Electrochemical detection of uric acid in mixed and clinical samples: a review. *Electroanalysis* **2011**, *23* (2), 305−320.
(41) Goyal, R. N.; Brajter-Toth, A.; Dryhurst, G. Futher insights into the electrochemical oxidation of uric acid. *J. Electroanal. Chem. Interfacial Electrochem.* **1982**, *131*, 181−202.
(42) Weber, S. G.; Long, J. T. Detection limits and selectivity in electrochemical detectors. *Anal. Chem.* **1988**, *60* (15), 903A−913A.
(43) Nayak, P.; Kurra, N.; Xia, C.; Alshareef, H. N. Highly efficient laser scribed graphene electrodes for on-chip electrochemical sensing applications. *Adv. Electron. Mater.* **2016**, *2* (10), 1600185.

https://doi.org/10.1021/acsomega.5c11146
ACS Omega 2026, 11, 25139−25148

(44) Choudhury, S.; Zafar, S.; Deepak, D.; Panghal, A.; Lochab, B.; Roy, S. S. A surface modified laser-induced graphene based flexible biosensor for multiplexed sweat analysis. *J. Mater. Chem. B* **2024**, *13* (1), 274−287.
(45) Yang, Y. J.; Li, W. CTAB functionalized graphene oxide/multiwalled carbon nanotube composite modified electrode for the simultaneous determination of ascorbic acid, dopamine, uric acid and nitrite. *Biosens. Bioelectron.* **2014**, *56*, 300−306.
(46) Brulé, D.; Sarwar, G.; Savoie, L. Changes in serum and urinary uric acid levels in normal human subjects fed purine-rich foods containing different amounts of adenine and hypoxanthine. *J. Am. Coll. Nutr.* **1992**, *11* (3), 353−358.
(47) Kippen, I.; Klinenberg, J. R.; Weinberger, A.; Wilcox, W. R. Factors affecting urate solubility in vitro. *Ann. Rheum. Dis.* **1974**, *33* (4), 313.
(48) Iwata, H.; Nishio, S.; Yokoyama, M.; Matsumoto, A.; Takeuchi, M. Solubility of uric acid and supersaturation of monosodium urate: why is uric acid so highly soluble in urine? *J. Urol.* **1989**, *142* (4), 1095−1098.
(49) Wilcox, W. R.; Khalaf, A.; Weinberger, A.; Kippen, I.; Klinenberg, J. R. Solubility of uric acid and monosodium urate. *Med. Biol. Eng.* **1972**, *10* (4), 522−531.
(50) Amarnath, K.; Selvi Gopal, T.; Josephine Malathi, A. C.; Pandiaraj, S.; Alruwaili, M.; Alshammari, A.; Alodhayb, A. N.; Abeykoon, C.; Grace, A. N.; Kumar, V. G. Electrochemical detection of dopamine and uric acid with annealed metal-organic framework/MXene ($CuO/C/Ti_3C_2T_x$) nanosheet composites for neurotransmitter sensing. *ACS Appl. Nano Mater.* **2025**, *8* (24), 12661−12675.
(51) Sharifuzzaman, M.; Chhetry, A.; Zahed, M. A.; Yoon, S. H.; Park, C. I.; Zhang, S.; Chandra Barman, S.; Sharma, S.; Yoon, H.; Park, J. Y. Smart bandage with integrated multifunctional sensors based on MXene-functionalized porous graphene scaffold for chronic wound care management. *Biosens. Bioelectron.* **2020**, *169*, 112637.
(52) Barber, R.; Cameron, S.; Devine, A.; McCombe, A.; Kirsty Pourshahidi, L.; Cundell, J.; Roy, S.; Mathur, A.; Casimero, C.; Papakonstantinou, P.; et al. Laser induced graphene sensors for assessing pH: application to wound management. *Electrochem. Commun.* **2021**, *123*, 106914.
(53) Liao, J.; Zhang, X.; Sun, Z.; Chen, H.; Fu, J.; Si, H.; Ge, C.; Lin, S. Laser-induced graphene-based wearable epidermal ion-selective sensors for noninvasive multiplexed sweat analysis. *Biosensors* **2022**, *12* (6), 397.
(54) Joshi, A.; Slaughter, G. Cost-effective hierarchical cobalt nanostructured laser-induced graphene for enhanced uric acid detection. *Adv. Sensor Res.* **2025**, *4*, No. e70003.
(55) Nong, J.; Zhang, N.; Wen, A.; Hu, C. Anti-biofouling laser-scribed graphene electrochemical sensor for reliable detection of uric acid in human saliva. *J. Electroanal. Chem.* **2024**, *952*, 117982.
(56) Yang, L.; Wang, H.; Abdullah, A. M.; Meng, C.; Chen, X.; Feng, A.; Cheng, H. Direct laser writing of the porous graphene foam for multiplexed electrochemical sweat sensors. *ACS Appl. Mater. Interfaces* **2023**, *15* (29), 34332−34342.
(57) Anshori, I.; Adzkia, A. R.; Harimurti, S.; Harimurti, S.; Handayani, N.; Suendo, V.; Zulfikar, M. A.; Klamchuen, A.; Chang, C. Y.; Handayani, M. Uric acid electrochemical biosensor based on a laser-induced graphene electrode modified with a honey-mediated nanocomposite of reduced graphene oxide and bimetallic silver−cobalt. *RSC Adv.* **2025**, *15* (47), 39431−39442.

https://doi.org/10.1021/acsomega.5c11146
ACS Omega 2026, 11, 25139−25148